The Astrophysical Journal, 819:81 (14pp), 2016 March 1 doi:10.3847/0004-637X/819/1/81

LYMAN CONTINUUM ESCAPE FRACTION OF STAR-FORMING DWARF GALAXIES AT $z \sim 1$

Michael J. Rutkowski[1], Claudia Scarlata[1], Francesco Haardt[2], Brian Siana[3], Alaina Henry[4,9], Marc Rafelski[4,9], Matthew Hayes[5], Mara Salvato[6], Anthony J. Pahl[1], Vihang Mehta[1], Melanie Beck[1], Matthew Malkan[7], and Harry I. Teplitz[8]

[1] Minnesota Institute for Astrophysics, University of Minnesota, 116 Church St. SE, Minneapolis, MN 55455, USA; rutkowsk@astro.umn.edu
[2] Dipartimento di Scienza e alta Tecnologia, Università dell'Insubria, via Valleggio 11, I-22100 Como, Italy
[3] Department of Physics and Astronomy, University of California, Riverside, CA 92521, USA
[4] Astrophysics Science Division, Goddard Space Flight Center, Code 665, Greenbelt, MD 20771, USA
[5] Department of Astronomy, Oskar Klein Centre, Stockholm University, AlbaNova University Centre, SE-106 91 Stockholm, Sweden
[6] Max Planck Institut für Plasma Physik and Excellence Cluster, D-85748 Garching, Germany
[7] Astronomy Division, University of California, Los Angeles, CA 90095-1562 USA
[8] Infrared Processing and Analysis Center, MS 100-22, Caltech, Pasadena, CA 91125, USA
Received 2015 April 18; accepted 2016 January 1; published 2016 March 1

ABSTRACT

To date, no direct detection of Lyman continuum emission has been measured for intermediate-redshift ($z \sim 1$) star-forming galaxies. We combine *Hubble Space Telescope* grism spectroscopy with *GALEX* UV and ground-based optical imaging to extend the search for escaping Lyman continuum to a large (~600) sample of $z \sim 1$ low-mass ($\log(\overline{M}) \simeq 9.3 M_{\odot}$), moderately star-forming ($\overline{\Psi} \lesssim 10 M_{\odot}\,\mathrm{yr}^{-1}$) galaxies selected initially on Hα emission. The characteristic escape fraction of LyC from star-forming galaxies (SFGs) that populate this parameter space remains weakly constrained by previous surveys, but these faint (sub-$L_{\star}$) SFGs are assumed to play a significant role in the reionization of neutral hydrogen in the intergalactic medium (IGM) at high redshift $z > 6$. We do not make an unambiguous detection of escaping LyC radiation from this $z \sim 1$ sample, individual non-detections to constrain the absolute Lyman continuum escape fraction, $f_{\mathrm{esc}} < 2.1\%$ (3σ). We measure an upper limit of $f_{\mathrm{esc}} < 9.6\%$ from a sample of SFGs selected on high Hα equivalent width (EW > 200 Å), which are thought to be close analogs of high redshift sources of reionization. For reference, we also present an emissivity-weighted escape fraction that is useful for measuring the general contribution SFGs to the ionizing UV background. In the discussion, we consider the implications of these intermediate redshift constraints for the reionization of hydrogen in the IGM at high ($z > 6$) redshift. If we assume our $z \sim 1$ SFGs, for which we measure this emissivity-weighted f_{esc}, are analogs to the high redshift sources of reionization, we find it is difficult to reconcile reionization by faint ($M_{\mathrm{UV}} \lesssim -13$) SFGs with a low escape fraction ($f_{\mathrm{esc}} < 3\%$), with constraints from independent high redshift observations. If f_{esc} evolves with redshift, reionization by SFGs may be consistent with observations from Planck.

Key words: galaxies: dwarf – galaxies: starburst – galaxies: star formation – ultraviolet: galaxies

1. INTRODUCTION

Hydrogen in the intergalactic medium (IGM) is ionized by the far-UV background of Lyman continuum photons (LyC, $\lambda < 912$ Å), in a process (called reionization) that began at $z > 10$ (Planck Collaboration et al. 2015) and was complete by $z \sim 6$ (Becker et al. 2001; Djorgovski et al. 2001; Fan et al. 2002; Siana 2005). Star-forming galaxies (SFGs), quasars (QSOs), and active galactic nuclei (AGNs) are considered the most likely sources of this emission (see the review by Loeb & Barkana 2001). However, at $z \lesssim 3$, QSO alone are sufficient to maintain the ionized state of the IGM (Haardt & Madau 1996, 2012; Rauch et al. 1997). At $z \gtrsim 3$, the space density of QSOs declines significantly (Osmer 1982; Siana 2005; Faucher-Giguére et al. 2008), implying an alternative source—presumably SFGs, and possibly low-luminosity AGNs (Giallongo et al. 2015)—must ultimately have completed reionization. This assumption must be confirmed observationally, or additional exotic sources of ionizing radiation must be invoked to explain the onset of reionization—e.g., dark matter annihilation in PopIII stars, accretion shocks in massive halos, or mini quasars (e.g., Zaroubi et al. 2007; Schleicher et al. 2009; Dopita et al. 2011, respectively).

If galaxies are to ionize hydrogen in the IGM, then it is necessary that these galaxies must (1) produce sufficient LyC photons in star-forming regions and (2) these photons must escape the emitting galaxy's interstellar medium (ISM). Although the first requirement will be met if star forming galaxies exist in sufficient numbers, the second requires that the column density of neutral hydrogen and dust in the ISM be relatively low.

Because the universe is opaque to LyC radiation at $z \gtrsim 4$ (Inoue & Iwata 2008; Inoue et al. 2014), direct measurements of the escape of ionizing photons, f_{esc}, can only be made for low to intermediate redshift SFGs. Thus, our understanding of the galaxies that initiated reionization at $z > 6$ must be informed by the study of their lower redshift analogs. The measurement of f_{esc} for low redshift SFGs has proven difficult, though. In the local universe, Tol-1247-232 (Leitet et al. 2013) and J0921+4509 (Borthakur et al. 2014) are observed to emit at LyC wavelengths, with the absolute escape fraction of ionizing photons from young, hot stars less than ~5%. A third galaxy, Haro 11, is also likely a LyC emitter but debated (Bergvall et al. 2006; Leitet et al. 2011; cf. Grimes et al. 2007).

Despite significant efforts with space-based observatories at $z \sim 1$, where the mean IGM opacity to LyC is still less than ~50%, no direct detection of escaping LyC from SFGs has been observed using the Hopkins UV Telescope (Leitherer

[9] NASA Post-doctoral Program Fellow.

et al. 1995), the *Hubble Space Telescope* (*HST*) Solar Blind Channel (Malkan et al. 2003; Siana et al. 2007, 2010; Bridge et al. 2010), or *GALEX* (Cowie et al. 2009; hereafter CBT09). At higher redshift ($z \sim 3$) the statistics appear to improve—Iwata et al. (2009), Nestor et al. (2011), and Mostardi et al. (2013) have reported $f_{\rm esc} \simeq 5\%$–7%. Yet, claims of direct detection of LyC emission from $z \sim 3$ SFGs remain tentative. *HST* imaging of LyC candidates selected from ground-based surveys often finds these galaxies to be contaminated by (non-ionizing) UV emission from low-redshift interlopers (Siana et al. 2015). Recently, Mostardi et al. (2015) confirmed 1 (of 16) candidate as a LyC emitter combining ground- and space-based imaging and spectroscopy and determined $f_{\rm esc} \lesssim 15\%$, marginally consistent with previous measurements at similar redshifts.

Recently, simulations have demonstrated that metal-poor, low-mass galaxies undergoing a strong episode of star formation may have a high escape fraction (Wise et al. 2014). In these low mass galaxies, supernova feedback may drive outflows, which clear sight-lines for LyC escape (Fujita et al. 2003; Razoumov & Sommer-Larsen 2006). Nevertheless, LyC studies require extremely deep observations because the non-ionizing to ionizing flux (f_ν) ratio is of the order ~3–10, depending on model assumptions. Previous studies at high redshifts focused on relatively massive galaxies (e.g., $M \gtrsim 10^{9.5}\ M_\odot$, Siana et al. 2010) with high UV luminosities. Here, we use a combination of *GALEX* and *HST* archival data, to study the ionizing emissivity in a large sample of SFGs selected at $z \sim 1$ via their Hα emission line. The average stellar mass for our full sample is $\overline{M} = 10^{9.3}\ M_\odot$, almost an order of magnitude lower than considered in previous studies of $f_{\rm esc}$ for $z \sim 1$ SFGs massive than previous studies. The size of the sample allows us to explore the dependency of the LyC escape on various galaxy properties: Hα equivalent width, orientation with respect to the observer, and stellar mass.

The paper is organized as follows. Section 2 presents the *HST* and *GALEX* observations, and the reduction of the data. Section 3 we discuss the steps involved in the selection of our robust sample of isolated galaxies, and define the sub-samples used in the analysis of the LyC escape fraction. In Section 4 we perform a stacking analysis and compute upper limits to $f_{\rm esc}$. Finally, we discuss the implications of these results for reionization in Section 5.

Throughout, we assume a ΛCDM cosmology with $\Omega_m = 0.27$, $\Omega_\Lambda = 0.73$, and $H_0 = 70\ {\rm km\ s^{-1}\ Mpc^{-1}}$ (Komatsu et al. 2011), and quote all fluxes on the AB magnitude system (Oke & Gunn 1983).

2. OBSERVATIONS

In this work we study the escape fraction of ionizing radiation from low-mass galaxies at $z \sim 1$. The sample is selected using archival IR grism spectroscopy over four deep fields—COSMOS, GOODS-North and South, and AEGIS—obtained as part of the 3DHST (PI: P. van Dokkum) and AGHAST (PI: B. Weiner) surveys. For the measurement of escaping LyC radiation we exploit the deep *GALEX* UV imaging ($m \simeq 27$ mag) available in these fields. Here, we discuss the pertinent details associated with the reduction of these data.

2.1. HST Data Reduction

We performed an independent reduction of the 3DHST WFC3/IR grism (G141) and direct (F140W) images obtained from the Milkulski Archive for Space Telescopes (MAST) archive, using a pipeline of processing software originally developed for the *WFC3 IR Spectroscopic Parallel* survey (WISP; PI: Malkan). For a full review of the pipeline, we refer the reader to Atek et al. (2010). Here we summarize key reduction stages in the processing of these 3DHST data, with specific details provided when modifications to the original (WISP) pipeline were required.

The 3DHST program observed ~500 sq. arcminutes comprised of ~28 unique pointings in each four deep fields. Each pointing was uniformly observed with an exposure time of 800 (F140W, direct image) and 4700 (G141, dispersed image) seconds. Each pointing consists of individual exposures obtained using a four-point dither pattern to improve the sampling of the (under-sampled) WFC3 IR point-spread function (PSF) and the rejection of cosmic rays and bad pixels. We used Astrodrizzle implemented via DrizzlePac (Gonzaga et al. 2012) to produce drizzled direct image "mosaics" for each of the unique pointings. We adopted a final pixel fraction parameter, pixfrac = 0.8, and pixel scale direct images with a scale of 0.″064 per pixel (Nyquist sampled) following Brammer et al. (2012). Sky subtraction of the direct images was performed "on the fly" as in the WISP pipeline. A master sky background developed by Atek et al. was applied for the background subtraction in individual G141 grism images. As noted in Brammer et al. (2012), grism data associated with nine pointings in GOODS-N suffer from a strong sky gradients. These data can be corrected with higher-order background sky models (see Brammer et al. 2012). We elected to remove the fields from further reduction in the pipeline because such extreme sky gradients affect only ~10% of all 3DHST fields.

We first measured positions and fluxes of sources for each direct image mosaic using Source Extractor (*SExtractor*; Bertins & Arnouts 1996). We then used the aXe software to produce input object lists of source coordinates for objects in the direct images, and projected these sources to guide the removal of contaminants and the extraction of object spectra from individual grism images. Individual extracted spectra for each G141 image were then combined using aXeDrizzle tasks to produce a catalog of one- and two-dimensional spectra for each unique pointing.

2.2. GALEX Images

At $z \sim 1$, ionizing and non-ionizing radiation are probed by *GALEX* FUV and NUV filters, respectively (see CBT09). We searched the MAST Archive[10] for GALEX primary guest investigator programs that observed the 3DHST fields for more than 10 ks in the FUV filter. Due to the total number of observations for each deep field with *GALEX*, these data have been prepared as individual coadded stacks. From the Archive, we downloaded these high-level, 1.25 deg^2 science mosaic frames (in units of counts s^{-1}), and exposure map frames ("rrhr" frames, which define the effective exposure time per pixel and account for detector variations). For each field we median combined all available exposures, using the exposure map frames as weight images. The total effective exposure time

[10] Maintained by the Space Telescope Science Institute and available online at http://galex.stsci.edu/GR6/.

Table 1
Archival *GALEX* FUV Imaging

Field	N_{gal}	t_{eff}(ks)	$\bar{m}_{FUV,sky}$
AEGIS	219	146	27.2
COSMOS	132	206	27.4
GOODS-N	113	126	27.1
GOODS-S	198	104	27.2

Note. Column 2: Number of galaxies, per field. Column 3: Effective exposure time, in ks, per galaxy. Column 4: 3σ FUV magnitude limit computed in a aperture with a radius equal to $0.67 \times 4\farcs5$.

in the FUV range in the 3DHST fields between 100 and 200 ks, because of the different number of programs observing each field. We converted the mosaics from detector units of (counts s^{-1}) to flux density units (erg s^{-1} cm^{-2} Hz^{-1}), assuming the photometric zero points of $m_{FUV,0} = 18.82$ and $m_{NUV,0} = 20.08$, measured in Cowie et al. (2009).

We computed the depth of each deep image by placing 10^4 apertures over the field of view and measuring the total flux within a $\sim 6''$ diameter. This diameter corresponds to a radius $0.673 \times FWHM_{PSF}$ (where $FWHM_{FUV} = 4\farcs5$, see Martin et al. 2003; Morrissey et al. 2007), and optimizes the signal-to-noise ratio (S/N), under the assumption of a Gaussian PSF. In Table 1 we present the 3σ magnitude limit in the *GALEX* FUV images, using the standard deviation of the Gaussian function that best fits the aperture flux distribution.

3. IDENTIFICATION OF $0.9 < z < 1.4$ EMISSION LINE GALAXIES

For each unique pointing in the 3DHST fields we produced a catalog of spectra that were then inspected by two co-authors independently to identify emission line galaxies (ELGs). At the resolution and typical S/N of the 3DHST grism spectra only bright emission lines are observed for $z \sim 1$ SFGs (e.g., [O III] and Hα). When multiple emission lines are present, the line identification—which is then used to measure an accurate grism spectroscopic redshift—is straightforward. When only a single emission is observed, the user defaulted the classification of the line to Hα, unless the line profile (asymmetric blue profile, in a compact source) was suggestive of the [O III] and Hβ emission line complex. To ensure robust spectroscopic redshifts measured from the grism spectra, we retained in the catalog all SFGs that met the following two requirements. First, we consider only galaxies for which the independent line-identifications agreed on the designation of the line (see Ross et al. 2015 for further details as they pertain to the WISP data reduction pipeline). Second, we included in the catalog only those sources for which photometric and spectroscopic redshifts agreed ($\Delta(z) = \frac{z_{spec} - z_{phot}}{1 + z_{phot}} \lesssim 5\%$). The reference photometric redshift, z_{phot}, used here for comparison with our measured grism redshift for each galaxy was drawn from the public photometric redshift catalogs[11] produced by the 3DHST team (Skelton et al. 2014).

Our spectroscopic redshifts measurements agreed with the photometric redshift for approximately 50% of all ELGs. This fraction improves to 70% when the photometric redshift catalogs produced by the 3DHST collaboration are used to correct for mis-classified single emission lines. Yet, approximately $\sim$30% of all ELGs were measured to have spectroscopic redshifts which disagreed with the photometric redshift. We discuss the likely causes for the remaining 30% of SFGs with discrepant redshifts in the Appendix A. We adopt a very conservative strategy in grism spectroscopic redshift selection and exclude all SFGs with discrepant spectroscopic redshifts that could not be corrected for the mis-classification of the emission line. With this cut, we produced our initial catalog of $\sim$1400 SFGs at $0.9 < z < 1.4$.

[11] Available online from http://3dhst.research.yale.edu/Data.php

4. SAMPLE SELECTION

When measuring the ionizing radiation below 912 Å, particular care has to be taken in selecting star-forming galaxies at the proper redshift. First, we remove AGNs from the sample, which we will consider independently in a future publication. We used public photometric redshift catalogs of AGN candidates identified by X-ray and optical-IR matched surveys of the AEGIS (Laird et al. 2009), GOODS-South and North (Alexander et al. 2003), and COSMOS (Salvato et al. 2011) fields. Second, we selected star-forming galaxies at $0.9 < z < 1.4$. The lower limit in redshift is fixed by the transmission curve of the *GALEX* FUV filter. The transmission drops below 5% at $\lambda > 1787$ Å (Morrissey et al. 2007), ensuring that for SFGs at $z > 0.9$ the *GALEX* FUV photometry is not significantly affected by non-ionizing emission (see CBT09). In addition, we remove all SFGs with Hα equivalent width measured to be less than 40 Å, a threshold below which the G141 grism data are likely to be significantly incomplete (<80%; see Colbert et al. 2013).

We also apply multiple selection criteria to select for isolated SFGs. This is in part necessary due to the coarse *GALEX* UV spatial resolution. The FUV *GALEX* PSF is $\sim 4\farcs5$, much larger than the spatial resolution reached with *HST*. Consequently, lower redshift galaxies in close spatial proximity to the ELGs of interest may irreducibly contaminate the photometry of the rest-frame LyC. In the following section, we discuss the additional selection criteria aiming at identifying a sample of isolated SFGs.

First, we identify isolated SFGs applying the same selection criteria applied by CBT09. Specifically, we remove any galaxy within $16\farcs0$ of a galaxy or star brighter than FUV = 23 or within $8\farcs0$ of a $23 < FUV < 25$ galaxy. In both instances, only those galaxies at $z < 0.7$ are considered. To measure photometry for sources in the *GALEX* imaging, we used *SExtractor* in dual-image mode, with the detection made in the NUV band. These criteria select from the initial sample a subset of 1050 ($\sim$80%) $0.9 < z < 1.4$ ELGs. For reference, this sample is $\sim 1.5\times$ larger than that considered by CBT09.

A visual inspection reveals that galaxies selected by the CBT09 criteria alone may still be in close proximity to other potentially low-redshift sources, making the unambiguous measurement of LyC photometry for the SFGs in the sample difficult (see Figure 2). Thus, we make a third and more stringent selection against SFGs with nearby neighbors, removing *all* SFGs with sources at $z < 0.9$ within $3\farcs0$.

Together these criteria define our "Grade A" sample, containing 618 SFGs. The 1050 SFGs selected with the CBT09 criteria will be referred to as the "Grade B" sample in the following analysis. We provide the number of Grade A and B galaxies in each field in Table 1. The emission line selection we used to identify the galaxy sample enables us to identify a large number of dwarf galaxies, in a mass range (50% of the

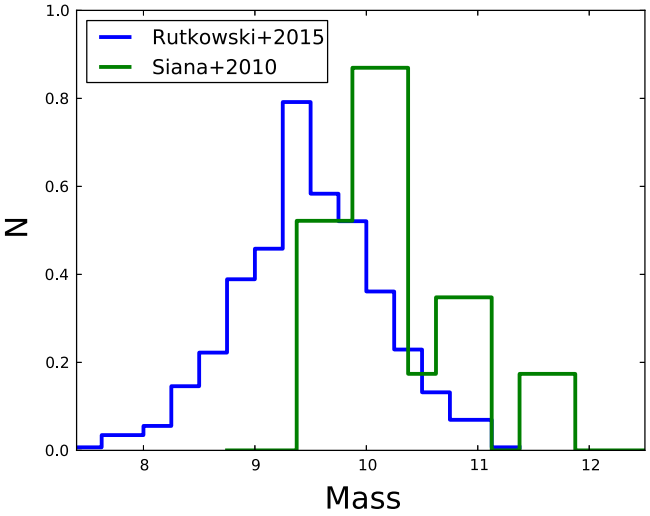

Figure 1. Normalized distribution of stellar masses for the Grade A sample (blue). Illustrated for comparison are the normalized distributions of stellar mass for the Siana et al. (2010) $z \sim 1$ sample of SFGs (green). Our selection on emission-line galaxies, in contrast to, e.g., the strength of the non-ionizing UV continuum, is largely insensitive to the stellar mass of the galaxy. Thus, we are able to extend the search for escaping LyC from $z \sim 1$ SFGs to significantly lower stellar masses than previously considered. For example, the median mass of the Grade A SFGs equals $10^{9.3}[M_{\odot}]$; ~50% of these galaxies are more than an order of magnitude *less massive* than considered in previous work.

sample is below $M = 10^9\ M_{\odot}$; see Figure 1) that can be as much as ~1.5 dex *lower* than the characteristic stellar mass of $z \sim 1$ SFGs (e.g., van der Burg et al. 2013).

With the large sample size of Grade A SFGs we define three sub-samples, each including hundreds of galaxies (see Table 2), with similar physical characteristics. Comparisons of $f_{\rm esc}$ measured for galaxies between these sub-samples may allow us to probe in unique an novel ways the efficiency with which ionizing photons escape from SFGs.

1. Hα Equivalent Width—We identify "extreme emission line" galaxies (EELGs; see Atek et al. 2011), requiring rest-frame $\mathrm{EW_{H\alpha}} \geqslant 200$ Å. These galaxies populate a unique parameter space in the study of LyC escape in which strong starbursts necessarily occur in relatively shallow gravitational potentials. These data will provide the first constraints on $f_{\rm esc}$ for such galaxies at this redshift range.
2. Orientation—We distinguish face-on galaxies from the full sample of Grade A SFGs using the ellipticity measured in the F140W band. We use the major-to-minor axis ratio criteria, $1 - \frac{b}{a} < 0.15$, which is a good proxy for inclination angle (Maller et al. 2009) to identify edge/face-on SFGs. A distinction between $f_{\rm esc}$ measured between these two classes can provide a direct test whether LyC photons escape isotropically from the disk or instead preferentially through channels in the ISM.
3. Stellar Mass or Luminosity—We select equally sized samples of low, medium and high ($\bar{M} \simeq 8.9$, 9.5 and 10.5 $M_{\odot}$, respectively) mass SFGs, using stellar masses reported in the 3DHST catalogs. Similarly, we define three bins in luminosity with the median absolute magnitude of each bin equal to −17.1, −18.1, and −18.9. Dahlen et al. (2007) report a characteristic UV magnitude for the $z \sim 1$ UV luminosity function (LF) equal to $M^* = 19.98$ mag; thus the median UV magnitudes of these three bins are equivalent to 0.07, 0.18, and 0.37 $\times L^*$.

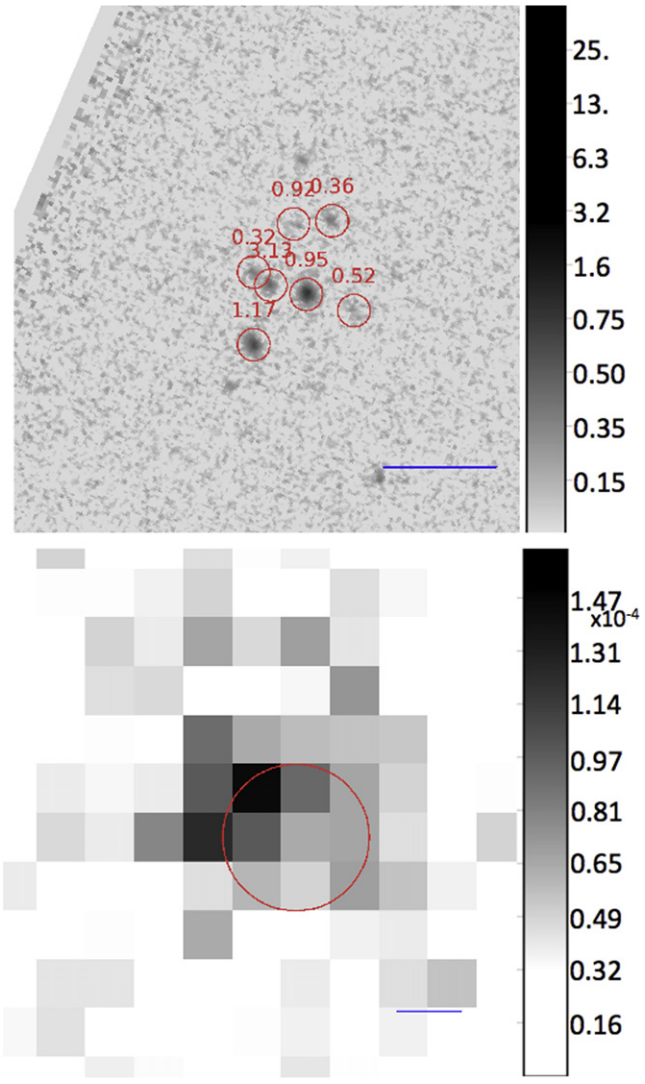

Figure 2. Approximately 30% of the ELGs identified by the CBT09 selection criteria are in close spatial proximity to low-redshift ($z < 0.9$) galaxies which may contaminate the UV photometry. Here we illustrate an galaxy in the COSMOS field, J100021.96+021545.6. In the upper panel is shown a $9'' \times 9''$ logarithmically scaled *HST* F140W postage stamp, centered on the $z = 0.95$ SFG. Overplotted are red regions ($r = 0''.5$) identifying sources identified in close proximity, with the labels indicating the galaxy's photometric redshift. Similarly in the lower panel, the corresponding *GALEX* FUV postage stamp is illustrated. Here, a red region ($r = 2''.25$; $0.5\times$ the *GALEX* FUV $4''.5$ FWHM) is centered on the position of the galaxy. In both panels the blue scale bar has a fixed length of $2''.0$ and units are cts s^{-1}.

The correlation between these characteristics and the detection (or lack of) of escaping LyC emission enhances our understanding of the physics of LyC escape. Here, we qualify each of these characteristics and their use in better revealing those factors affecting the escape of LyC from SFGs.

First, EELGs are defined on the basis of their high emission-line equivalent widths, indicative of a recent episode of star formation. EELGs are characterized by high specific star-formation rates ($\gtrsim 10^{-8}$ yr^{-1}), and may be offset by as much as ~1 dex from the "star-forming" main-sequence of galaxies at $z \sim 1$ (Atek et al. 2011; Wuyts et al. 2011; Amorin et al. 2014).

Table 2
Upper limits to f_{esc} at $z \sim 1$, Measured Quantities

Selection	N_{gal}	$\bar{f}_U$ ($\bar{m}_U$)[a] (jy (mag))	$\bar{f}_{LyC}$ ($\bar{m}_{LyC}$)[a] (jy (mag))	$\left(\frac{L_{UV}}{L_{LyC}}\right)_{obs}$	$\left(\frac{L_{UV}}{L_{LyC}}\right)_{IGM,corr}$	$\left(\frac{L_{LyC}}{L_{UV}}\right)_{obs}$	$\left(\frac{L_{LyC}}{L_{UV}}\right)_{IGM,corr}$
Grade A	618	6.5×10^{-7} (24.43)	2.7×10^{-9} (30.42)	235.1	129.3	4.2×10^{-3}	0.7×10^{-2}
Grade B	997	6.5×10^{-7} (24.44)	2.1×10^{-9} (30.68)	295.8	162.7	3.3×10^{-3}	0.6×10^{-2}
Edge-On	455	6.3×10^{-7} (24.47)	3.2×10^{-9} (30.26)	195.8	107.6	5.1×10^{-3}	0.9×10^{-2}
Face-On	118	7.4×10^{-7} (24.29)	5.9×10^{-9} (29.60)	125.1	68.83	7.9×10^{-3}	1.4×10^{-2}
High Mass	206	7.9×10^{-7} (24.22)	4.8×10^{-9} (29.82)	164.9	90.72	6.0×10^{-3}	1.1×10^{-2}
Med. Mass	…	7.3×10^{-7} (24.31)	4.7×10^{-9} (29.84)	154.5	85.01	6.4×10^{-3}	1.1×10^{-2}
Low Mass	…	4.3×10^{-7} (24.87)	4.6×10^{-9} (29.86)	93.83	51.61	10.6×10^{-3}	1.9×10^{-2}
High EW	72	6.5×10^{-7} (24.43)	7.4×10^{-9} (29.35)	88.26	48.54	11.3×10^{-3}	2.0×10^{-2}
Bright M_{UV}	206	1.1×10^{-7} (23.80)	4.7×10^{-9} (29.83)	245.4	135.0	4.0×10^{-3}	0.7×10^{-2}
Med. M_{UV}	…	5.4×10^{-7} (24.63)	4.7×10^{-9} (29.85)	115.1	63.31	8.6×10^{-3}	1.5×10^{-2}
Faint M_{UV}	…	2.4×10^{-7} (25.50)	4.6×10^{-9} (29.87)	53.10	29.20	18.8×10^{-3}	3.4×10^{-2}

Note. Here we accumulate measured upper limits (3σ) which are directly measured from the UV photometry. Column entries are defined as follows: Column 1: Sample Selection criteria (see Section 4). Column 2: Number of galaxies included in each galaxy. The mass and luminosity sub-samples were selected to have equal numbers of galaxy per bin. Columns 3, 5: The observed UV continuum ratios. Columns 4, 6: The UV continuum ratios corrected for a mean transmission of the IGM of 55% at $z \sim 1$ (Section 7). We note that although the Grade A sample includes nearly the same number of SFGs (618 versus 626) considered in CBT09, the upper limits presented here for the LyC luminosity are ∼50% deeper due to the availability of ∼5 years of well-calibrated deeper, co-added images than were available in the MAST archive for that novel study of the escape of LyC at $z \sim 1$ in UV archival images.

At high redshift, EELGs have been observed to likely emit LyC emitters (de Barros et al. 2016) and thus are of interest to consider in this work specifically. Specifically, extreme Hα-ELGs are of interest, which can be detected in G141 at $z \sim 1$. At $z \sim 0.2$, Cowie et al. (2011) found ∼75% of Lyα emitters selected from *GALEX* grism observations to have EW (Hα) > 100 Å. More recently, Henry et al. (2015) observed 10 high EW, luminous compact SFGs with UV *HST* Cosmic Origins Spectrograph observations and found Lyα emission in 100% of the galaxies. Noting that neutral hydrogen is optically thick to Lyα at column densities 10^4 times *lower* than at the Lyman-limit, these observed correlations between Extreme-Hα ELGs and Lyα make EELGs appealing candidates in a search for escaping LyC emission.

The second criterion—galaxy inclination—seeks to characterize the role of anisotropic escape. Assuming that the LyC-emitting star-forming regions (cf., Kimm & Cen 2014) are sequestered to a gas-rich disk in the galaxy, the column of neutral gas and dust in the ISM is lowest in the direction normal to the disk. Channels through the attenuating medium are evacuated more easily perpendicularly to the disk. As a result, f_{esc} could show a dependence on the orientation of the disk relative to the observer.

The final selection criterion is designed to constrain f_{esc} as a function of UV luminosity, because it has been suggested that LyC may easily escape from low mass SFGs. In fact, the CANDELS survey demonstrates that the observed populations of SFGs at $z > 6$ do not, under reasonable assumptions, produce sufficient ionizing photons to maintain an ionized universe (e.g., Finkelstein et al. 2015; Robertson et al. 2015). To resolve this tension it has been suggested that f_{esc} is higher for low luminosity galaxies, and a population of very faint ($M_{UV} \lesssim -13$), yet unobserved galaxies with high $f_{esc} \gtrsim 20\%$ is typically invoked. Our sample probes two magnitudes fainter in the UV than previous studies at similar redshifts, thus allowing us to investigate any dependency of f_{esc} with M_{UV}. We refer the reader to Figure 2 for an illustration of the stellar masses to which we are sensitive with these data.

5. OBSERVED UV TO LYC FLUX RATIO

For each galaxy, we use ground-based *U*-band and *GALEX* FUV photometry to compute the observed non-ionizing (UV) to LyC flux ratio, $(L_{UV}/L_{LyC})_{obs}$. The 3σ magnitude limit of the LyC images (*GALEX* FUV) ranges between 27.4 and 27.1 (see Table 1). Thus, considering the average UV—LyC colors of known LyC leakers (see, e.g., Nestor et al. 2013, Mostardi et al. 2015), our survey is sensitive to LyC radiation in individual objects with rest-frame UV magnitude (i.e., *U*-band magnitude) brighter than 25.5. Thus, individual candidates may be detected in the *GALEX* FUV images sensitive to rest-frame LyC.

We first visually inspected all of the ELGs' *GALEX* FUV stamps to search for these potential individual detections, and find 6 ELGs selected using the CBT09 criteria (i.e., Grade B ELGs) are identified. We used Source Extractor in dual image mode—the corresponding stacked *GALEX* NUV images were used for the definition of the sources' Kron apertures—to confirm that each of these sources were detected at $\gtrsim 2.5\sigma$ in the LyC images. In each case, a comparison of these galaxies with the higher resolution *HST* F140W and ground-based *U*-band data,[12] strongly suggests that the flux is not associated with the SFG, but rather with a foreground galaxy in close proximity. No galaxies in the more robust Grade A sample are detected individually in the LyC image.

With no unambiguous individual object detected in LyC, we perform a stacking analysis, averaging the FUV images of all galaxies, as well as of the objects in the subsamples described in Section 4. When creating the stack for the Grade B sample, we removed those objects that had a spurious individual detection in the FUV. To prepare the stacks, we first produced equally sized postage FUV images centered on the SFG and then median combined all stamps, scaling the flux in each stamp by the position-dependent exposure time. For each subsample, we measured the total flux within an optimally sized aperture of radius $0.67 \times 4.''2$. In Table 3 we report the

[12] We use the native scale *U*-band images downloaded from the CADC archives at http://www4.cadc-ccda.hia-iha.nrc-cnrc.gc.ca/en/cfht/.

Table 3
Upper Limits to f_{esc} at $z \sim 1$, Derived Quantities

Selection	$f_{esc,rel}$	f_{esc}	$L_{H\alpha}$ (erg s^{-1})	Q_{ion} (photons s^{-1})	$\nu_{eff} L_{LyC,int}$ (erg s^{-1})	$\nu\ L_{LyC,obs}$ (erg s^{-1})	$f_{esc}^{H\alpha}$
Grade A	8.0%	2.1%	8.9×10^{41}	1.3×10^{54}	3.3×10^{43}	1.0×10^{42}	3.2%
Grade B	7.5%	1.9%	8.7×10^{41}	1.2×10^{54}	3.3×10^{43}	9.8×10^{41}	2.9%
Edge-On	8.5%	2.2%	8.6×10^{41}	1.2×10^{54}	3.2×10^{43}	1.1×10^{42}	3.3%
Face-On	120·%	2.6%	8.9×10^{41}	1.3×10^{54}	3.3×10^{43}	1.8×10^{42}	5.3%
High Mass	9.0%	0.7%	1.6×10^{42}	2.3×10^{54}	6.1×10^{43}	1.5×10^{42}	2.4%
Med. Mass	10.0%	3.2%	6.9×10^{41}	1.0×10^{54}	2.6×10^{43}	1.4×10^{42}	5.5%
Low Mass	15.8%	10.9%	4.3×10^{41}	6.3×10^{53}	1.6×10^{43}	1.4×10^{42}	9.0%
High EW	15.3%	9.6%	5.9×10^{41}	8.7×10^{53}	2.2×10^{43}	2.1×10^{42}	9.3%
Bright M_{UV}	5.8%	1.7%	1.4×10^{42}	2.0×10^{54}	5.4×10^{43}	1.5×10^{42}	2.7%
Med. M_{UV}	12.8%	3.9%	7.2×10^{41}	1.0×10^{54}	2.7×10^{43}	1.4×10^{42}	5.2%
Faint M_{UV}	27.5%	5.6%	5.9×10^{41}	8.7×10^{53}	2.2×10^{43}	1.4×10^{42}	6.1%

Note. The upper limits to f_{esc} derived from the ionizing to non-ionizing UV continuum with columns defined as follows: Column 1: Sample selection criteria (see Section 4) as in Table 2; Columns 2, 3: Upper limits to the escape fraction derived from the ratio of ionizing to non-ionizing continuum ratios. These data were measured assuming an intrinsic continuum ratio of 7. Please see Section 7.1.1 for a discussion of the range of plausible intrinsic ratios for young, star-forming galaxies;. Columns 4, 5: The intrinsic Hα luminosity and inferred rate of ionizing photons. As in Columns 2, 3 all quantities have been corrected for nebular dust extinction using the median stellar $E(B-V)$ measured by Skelton et al. (2014); Column 6: The intrinsic LyC as derived from the Hα luminosity; Column 7: The observed, dust and IGM corrected LyC luminosity measured from the *GALEX* FUV stacked images; Column 8: The upper limit to escaped derived by the new method presented in Section 7.2 from the LyC–Hα ratio.

3σ flux limits of the stacked FUV LyC images for each subsample. We find no significant detection, above 3σ, in the stacked images (see Figure 3).

At the redshift of our sample, the non-ionizing rest-frame 1500 Å continuum is covered by the *U*-band filter, which is minimally affected by Lyα emission and Lyα-forest absorption. For each subsample, we computed the median *U*-band flux density of all objects in the sample, and report the measurements in Table 3. All measurements in Table 2 are corrected for (minor) Milky Way extinction at non-ionizing and ionizing UV continuum wavelengths, using extinction laws defined by Cardelli et al. (1989) and O'Donnell (1994). We correct for Galactic extinction assuming a spatially uniform color excess specific to each field from the dust maps of Schlegel et al. (1998). In Figure 4, we compare the 3σ limit on the observed LyC-to-UV flux ratio, corrected for average attenuation along the line of sight ($(L_{UV}/L_{LyC})_{obs} \exp[\tau_{-HI,IGM}]$), computed for our Grade A and high-EW samples. For reference, we include the observed IGM corrected ratios from previous surveys of *individual* $z \sim 1$ galaxies. The large number of galaxies that enter in the calculation of the 3σ upper limits allow us to probe a factor of a few deeper in $(L_{UV}/L_{LyC})_{obs}$ than previous studies.

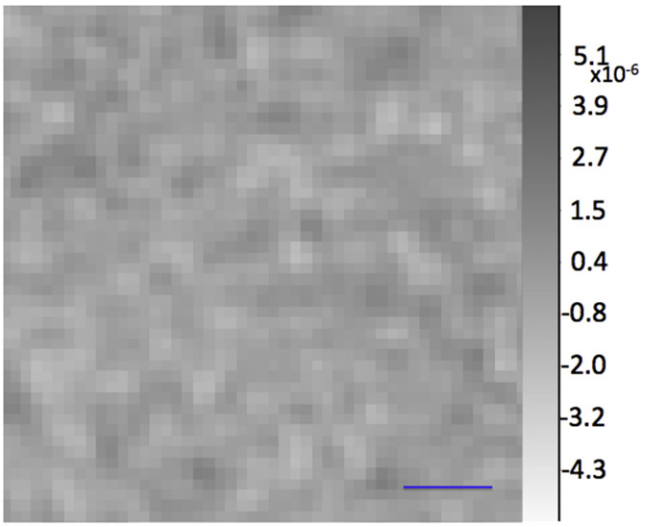

Figure 3. Grade A stacked *GALEX* FUV image of ELGs at $z \sim 1$, linearly scaled (cts s^{-1}) and smoothed with a σ = 2pix Gaussian kernel, shows no significant (3σ) emission. Note, the scalebar here has a length of 15″. We produce stacked images for all subsamples of ELGs listed in Table 2 and measure the variance in the sky background in 1000s of randomly placed circular apertures to determine upper limits to the LyC flux. The upper limits to relative escape fraction of LyC presented in Table 3 were the derived from these measurements.

6. THE LYC ESCAPE FRACTION

Lyman continuum emission produced by young, hot stars embedded in the gas-rich media of galaxies is attenuated by neutral hydrogen (both within and outside galaxies) and the dust associated with the ISM. The *absolute* fraction of LyC radiation escaping from a galaxy is defined as $f_{esc} \equiv \frac{L_{LyC,esc}}{L_{LyC,int}}$, where $L_{LyC,esc}$ is the ionizing luminosity attenuated by the gas and dust in the ISM, and $L_{LyC,int}$ is the intrinsic emissivity of the stars below 912 Å. At redshifts $z \gtrsim 0.4$, the contribution by the neutral IGM cannot be neglected and the observed luminosity below 912 Å can be written as $L_{LyC,obs} = L_{LyC,esc} \exp[-\tau_{HI,IGM}]$. With these definitions, the absolute escape fraction of ionizing radiation can be written in terms of the observed ionizing emissivity as

$$f_{esc} = \frac{L_{LyC,obs} \exp[\tau_{HI,IGM}]}{L_{LyC,int}}. \quad (1)$$

If the attenuation by the galaxy's neutral hydrogen and dust ($\exp[-\tau_{HI,ISM}]$ and $\exp[-\tau_{dust,\lambda}]$, respectively) were known, the absolute escape fraction could be written as

$$f_{esc} = \exp[-\tau_{HI,ISM}] \cdot \exp[-\tau_{dust,\lambda}]. \quad (2)$$

However, the dust extinction curve at wavelengths lower than 912 Å ($\tau_{dust,\lambda}$) is highly uncertain. Moreover, the attenuation of $L_{LyC,int}$ by neutral gas and dust (i.e., $\exp[-\tau_{HI,ISM}]$ and

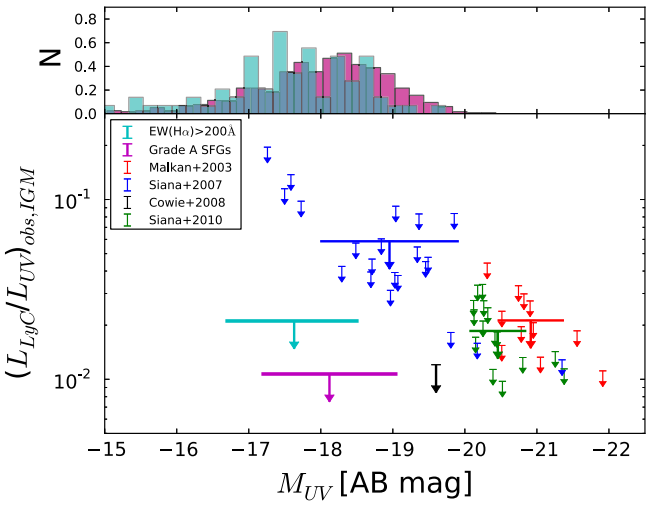

Figure 4. Observed LyC-to-UV flux ratio, corrected for IGM extinction, is provided here for the Grade A and High EW samples (violet and cyan, respectively). The range on the absolute magnitude provided indicates the 1σ width on the median for each sample, assuming the sample distribution is Gaussian. For reference, we also reproduce the upper limits measured for individual $z \sim 1$ SFGs from Malkan et al. (2003), and Siana et al. (2007, 2010) in red, green, and blue limits, respectively. Stacking *GALEX* FUV data enables us to place limits to the UV continuum ratio for $z \sim 1$ SFGs as good or better as in previous studies, and we can extend previous efforts (black, CBT09) to significantly fainter populations of SFGs.

$\exp[-\tau_{\mathrm{dust},\lambda}]$) within the SFG population varies strongly with the total gas and dust mass, the "patchiness" and distribution of gas and dust, and the orientation of the disk with respect to the observer. To overcome these uncertainties, Steidel et al. (2001) introduced the *relative* escape fraction, defined as

$$f_{\mathrm{esc,rel}} = f_{\mathrm{esc,rel}}^{\mathrm{LyC}} = \frac{(L_{\mathrm{UV}}/L_{\mathrm{LyC}})_{\mathrm{int}}}{(L_{\mathrm{UV}}/L_{\mathrm{LyC}})_{\mathrm{obs}}} \cdot \exp[\tau_{\mathrm{IGM}}], \quad (3)$$

corresponding to the fraction of emitted 900 Å photons that escapes the galaxy without being absorbed by interstellar medium divided by the fraction of non-ionizing (at 1500 Å) photons that escapes. Note that the relative escape fraction in Equation (3) is corrected for HI attenuation by the IGM. If the column density and redshift distributions of neutral absorbers were known, the opacity of the IGM along the line of sight could be modeled. However, because this is typically not the case, a statistical redshift-dependent correction is usually applied to derive $L_{\mathrm{LyC,esc}}$ from $L_{\mathrm{LyC,obs}}$ using the models of, e.g., Haardt & Madau 2012.

The relative escape fraction can be directly related to f_{esc}:

$$f_{\mathrm{esc}} = f_{\mathrm{esc,rel}} \cdot \exp[-\tau_{\mathrm{dust,UV}}], \quad (4)$$

where $\exp[-\tau_{\mathrm{dust,UV}}]$ is the attenuation of the non-ionizing UV continuum (typically measured at 1500 Å) by dust.

7. OBSERVATIONAL CONSTRAINTS ON THE ESCAPE FRACTION

7.1. Absolute f_{esc} from Relative f_{esc}

We use Equations (3) and (4) to compute upper limits on the relative and absolute escape fractions. The intrinsic $(L_{\mathrm{UV}}/L_{\mathrm{LyC}})_{\mathrm{int}}$ ratio is highly uncertain and depends on various properties of the stellar population (see discussion in Section 7.1.1). We assume an average value of $(L_{\mathrm{UV}}/L_{\mathrm{LyC}})_{\mathrm{int}} = 7$ (in L_ν). This value was computed from constant star-formation Starbust99 models, assuming a Salpeter initial mass function (IMF), solar metallicity and no stellar rotation. This ratio is consistent with what is typically assumed in the literature; e.g., Siana et al. (2010) use $(L_{\mathrm{UV}}/L_{\mathrm{LyC}})_{\mathrm{int}} \simeq 8$.

We compute the correction factor for absorption by the IGM ($\exp[\tau_{\mathrm{HI,IGM}}]$), from the piecewise parametrization of the distribution in redshifts and column density of intergalactic absorbers as described in Haardt & Madau (2012). We derive a mean IGM transmission at $\lambda < 912$ Å of $T \simeq 55\%$ (corresponding to $\exp[\tau_{\mathrm{IGM}}] \sim 1.8$), computed at the median redshift of our sample. We verified that the assumed value of the IGM opacity does not introduce systematics in our calculations: the redshift distribution is approximately flat in the 0.9–1.4 redshift range, and the attenuation changes by less than 5% at the two extrema of the redshift range. This small variation is the result of the shallow redshift dependency of the column density distribution of absorbers, which scales as $(1+z)^{0.16}$ in the redshift range $0 < z < 1.5$ (Weymann et al. 1998).

We report the relative escape fraction calculated assuming $(L_{\mathrm{UV}}/L_{\mathrm{LyC}})_{\mathrm{int}} = 7$ in Table 2; the range of possible values to this intrinsic ratio is discussed further in the Section 7.1.1. In order to compute the absolute escape fraction (f_{esc}) we need to correct the relative escape fraction for dust attenuation at 1500 Å. We computed an average attenuation for each group, using the stellar $E(B-V)_s$ provided by Skelton et al. (2014), assuming a Calzetti extinction law (Calzetti et al. 2000). The absolute escape fractions are also reported in Table 2.

7.1.1. The Intrinsic $(L_{\mathrm{UV}}/L_{\mathrm{LyC}})_{int}$ Ratio

The values of the absolute escape fraction reported in column 3 of Table 3 depend on two assumptions: the average IGM attenuation (discussed in the previous section) and the intrinsic UV-to-LyC ratio. Here, we discuss the systematic uncertainty in this intrinsic ratio arising from the choice of stellar models.

We have assumed $(L_{\mathrm{UV}}/L_{\mathrm{LyC}})_{\mathrm{int}} = 7$, consistent with previous studies in the literature. For a given star-formation history, this ratio depends strongly on, e.g., the age or "burstiness" of the stellar population (Dominguez et al. 2015), whether or not rotation is accounted for in the stellar libraries used to compute the synthetic spectra (Levesque et al. 2012; Leitherer et al. 2014). We have measured the systematic uncertainty associated with the assumption of a constant value, using a large library of galaxy spectra generated with two stellar population synthesis codes, *galaxev* (Bruzual & Charlot 2003) and *Starburst99* (Leitherer et al. 1999)[13] that incorporate a variety of stellar templates which have varied intrinsic LyC-to-UV continuum ratios as we will demonstrate below.

We consider the following models produced with *galexev*: 30 logarithmically spaced ages between 10^6—8×10^8 years, constant and exponentially declining SFHs ($\tau = 0.02$, 0.05, 0.2, 0.5, 1.0), Salpeter (1955) and Chabrier (2003) IMF, 5 metallicities ($Z = 0.005$, 0.02, 0.04, 1, $2.5 \times Z_\odot$), and Padova94 stellar evolution tracks. For the composite models generated with *Starburst99* we produce models with the same ages, constant star formation histories, solar metallicity,

[13] *Starburst99* is available online at: http://www.stsci.edu/science/starburst99/docs/default.htm.

Salpeter IMF and both Geneva and Ekström et al. (2012) evolutionary tracks. The latter tracks include a detailed treatment of stellar rotation effects, and the *Starburst99* library we used includes models with rotation speeds equal to no rotation and rotation speed equal to 40% of the break-up speed for stars on the zero-age main sequence. Furthermore, we include models with a top-heavy IMF slope ($\alpha = 1.7$ at $M_* > 0.5\ M_\odot$). For each model in the library we computed $(L_{\rm UV}/L_{\rm LyC})_{\rm int}$, and the results are summarized, as a function of the age of the stellar population, in Figure 5.

In Figure 5, we only show exponentially declining SFH models up to ages for which hot massive stars are still on the main sequence (i.e., age $< \tau + 25$ Myr). This is because galaxies in our sample were selected via the Hα emission line, implying the presence of ionized gas. For a given star formation history, and at any given age, the stellar metallicity is found to have a minor impact on the intrinsic ratio, introducing a scatter of the order of 20%. The largest uncertainty is introduced by our ignorance of the stellar age (more specifically, the age of the latest burst of star formation) and the IMF. Additionally, Figure 5 shows that the ratio can be affected by stellar rotation, which reduces the intrinsic UV-to-LyC ratio by approximately 20%–30% for a given IMF. Finally, we note that the choice of stellar templates libraries (*galexev* versus *Starburst99*) also affects the result, as shown by the comparison of the solid dark blue and orange curves in Figure 5.

Stellar population parameters can be derived using SED fitting techniques (e.g., Skelton et al. 2014). However, the resulting parameters, particularly stellar age and SFR, are affected by large systematic biases and uncertainties because of the assumed SFH may be a poor representation of the real SFH of a galaxy (see, e.g., Lee et al. 2009; Dominguez et al. 2015). Moreover, no constraints exist at high redshifts on the IMF in star-forming regions. For these reasons, and to allow the reader to compare our results directly with other similar studies, we adopt a conservative $(L_{\rm UV}/L_{\rm LyC})_{\rm int} = 7$, noting that the upper limits could be a factor of three *lower*, depending on the exact value assumed.

7.2. Absolute $f_{\rm esc}$ from Hα luminosity

The absolute escape fraction can also be computed directly (i.e., without first calculating $f_{\rm esc,rel}$) if the intrinsic ionizing emissivity can be estimated through indirect observations. By definition, for each galaxy in our samples we have a measurement of its rest-frame Hα luminosity, which can be used to estimate the amount of ionizing radiation absorbed by neutral hydrogen in the galaxy. For a luminosity-bounded H II region, the Hα luminosity produced by recombination is simply proportional to the rate of ionizing photons, i.e., $L_{\rm H\alpha} \propto Q_{\rm ion}$.

In galaxies, however, the situation is more complex. First, dust is known to be present inside H II regions, and absorbs $h\nu > 13.6$ eV photons that would otherwise be able to ionize hydrogen, thereby reducing the luminosity of the recombination lines. Defining $f_{\rm ion}$ as the fraction of ionizing photons absorbed by neutral hydrogen and $(1 - f_{\rm ion})$ the fraction of photons absorbed by dust in the galaxy, the intrinsic rate of ionizing photons produced in the galaxy can be written as $Q_{\rm ion}^{\rm int} = f_{\rm ion}\, Q_{\rm ion}^{\rm int} + (1 - f_{\rm ion}) Q_{\rm ion}^{\rm int}$. This equation assumes that the fraction of ionizing photons escaping from the galaxy is negligible, an assumption justified by the result in the previous section. The first term in the the expression for $Q_{\rm ion}^{\rm int}$ will result in hydrogen ionization and Hα-emission by recombination. The second term will result in thermal heating of the dust, and infrared re-emission, which will depend on the dust grain properties and distribution of the dust with respect to the ionizing sources. No constraints exist on $f_{\rm ion}$ in high redshift galaxies. In the local universe, however, Inoue (2002)

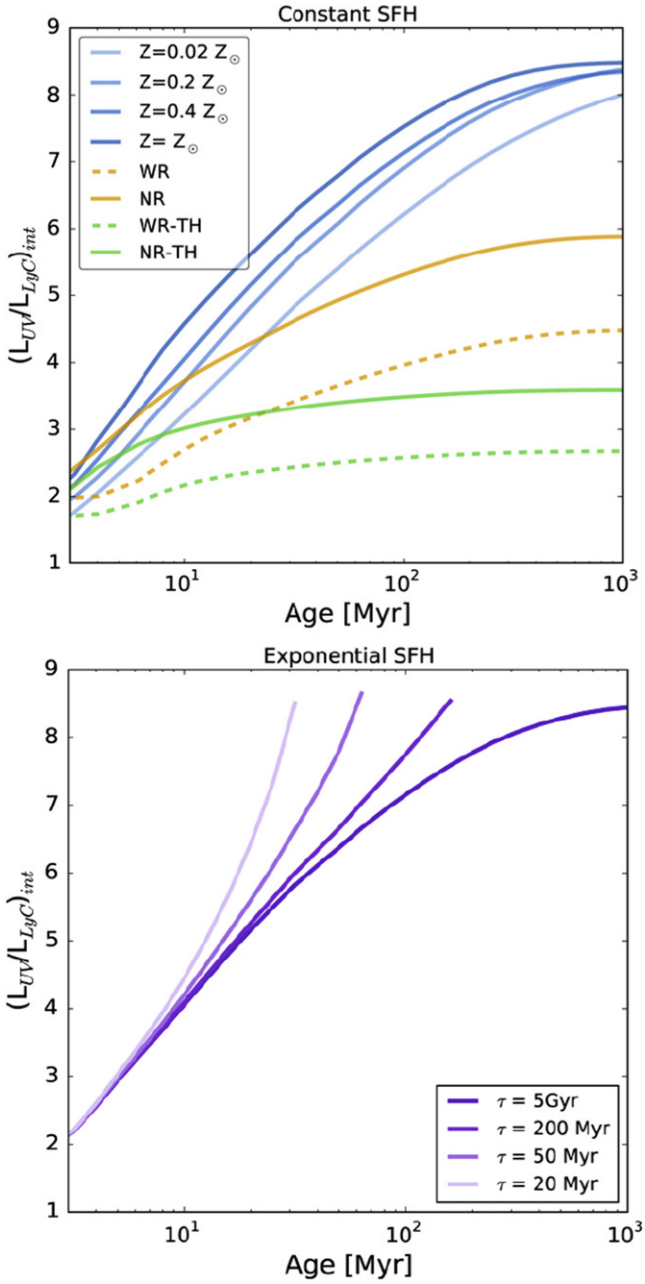

Figure 5. Variation of the intrinsic UV-to-LyC luminosity ratio as a function of the age of the stellar population and star formation history. In the upper figure, the ratios are derived from models assuming constant star formation and varying metallicity. Here, we reproduce (blue) the intrinsic ratio from *galexev* models with constant star formation, allowing the metallicity of the model to vary between 0.02 and $1 \times Z_\odot$. Additionally, we produce models using *Starburst99* for constant star formation history assuming a constant solar metallicity. In yellow, we illustrate the intrinsic ratio for models in which the rotation speed of massive, main sequence stars equals to zero and 40% of the break-speed. Furthermore, in green we illustrate the intrinsic ratio as a function of age for models with and without rotation assuming a top-heavy ($\alpha = -1.7$) IMF. In the lower figure, the intrinsic ratio is derived exclusively from *galexev* models assuming a range of exponentially declining SFHs.

measured $f_{\rm ion}$ in a sample of Galactic H II regions, using infrared and radio continuum observations. Because our observations measure the Hα luminosity integrated over all H II regions in the galaxy, we will assume that $f_{\rm ion} = 0.5$, i.e., the average value measured by Inoue (2002). With this assumption, we can compute the intrinsic rate of ionizing photons from the extinction-corrected Hα luminosity.

First, we correct the observed Hα luminosity for the contribution to N II, by applying an average correction that depends on the galaxy's stellar mass following Erb et al. (2006). To correct the Hα luminosity for dust extinction we used a mass-dependent correction defined in Dominguez et al. (2014) such that $A_{\rm H\alpha} = 3.3 \times E(B-V)_n$, where the color excess here equals to the nebular color excess computed from stellar color excess as $E(B-V)_n = 2.27 \times E(B-V)_s$ (see, e.g., Calzetti et al. 2000). We use the best-fit $E(B-V)_s$ provided by Skelton et al. (2014). Assuming the Calzetti extinction law, the extinction-corrected Hα luminosity is then $L^{\rm int}_{\rm H\alpha} = L_{\rm H\alpha} \times 10^{0.4E(B-V)_n k_{\tau \rm H\alpha}}$. We then obtain the intrinsic rate of ionizing photons from the unobscured Hα luminosity as $Q^{\rm int}_{\rm ion} = L^{\rm int}_{\rm H\alpha} f^{-1}_{\rm ion} c^{-1}_{\rm H\alpha}$, (where $c_{\rm H\alpha} = 1.37 \times 10^{-12}$ erg, see e.g., Schaerer 2003). Finally, we compute the intrinsic ionizing power from the rate of ionizing photons as $\nu L_{\rm LyC,int} = \epsilon_{\rm ion} Q^{\rm int}_{\rm ion}$, where $\epsilon_{\rm ion}$ is the average energy per ionizing photon computed from the same *Starburst99* model used in the previous section,[14] and $\epsilon_{\rm ion} = 16.2$ eV ($\lambda = 765$ Å).

For each group of galaxies, we compute the 3σ limits on the absolute escape fraction,[15] defined here as the ratio of the observed (corrected for IGM absorption) to intrinsic ionizing power:

$$f^{\rm H\alpha}_{\rm esc} = \frac{\nu_{\rm eff} L_{\rm LyC,obs} \exp[\tau_{\rm IGM}]}{\nu L_{\rm LyC,int}}, \quad (5)$$

where $\nu_{\rm eff}$ is computed from the pivot wavelength of the FUV filter, divided by the median redshift of each galaxy sample ($\langle z \rangle = 1.1$, for all sub-samples). The results, reported in the last column of Table 2, are in good agreement with the upper limits to $f_{\rm esc}$ measured from the UV-to-LyC continuum ratio. For example, for the Grade A sample $f_{\rm esc} < 2.1\%$, whereas $f^{\rm H\alpha}_{\rm esc} < 3.2\%$.

8. EMISSIVITY-WEIGHTED $f_{\rm esc}$

Theoretical models of reionization assume a constant value of the absolute escape fraction as a function of galaxy UV luminosity. Here, we compute an emissivity-weighted $f_{\rm esc}$ limit, that can be used to predict the number of ionizing photons for an observed non-ionizing UV luminosity function (LF). We define the emissivity-weighted $f_{\rm esc}$ limit as:

$$\langle f_{\rm esc} \rangle = \frac{\int_{L_{\rm min}}^{L_{\rm max}} f_{\rm esc} \cdot L \cdot \phi(L) dL}{\int_{L_{\rm min}}^{L_{\rm max}} L \cdot \phi(L) dL}, \quad (6)$$

[14] The average energy per ionizing photon is computed from the *Starburst99* template $L(\nu)$ spectrum as $\epsilon_{\rm ion} = \frac{\int_{\nu_c}^{\infty} L(\nu) d\nu}{\int_{\nu_c}^{\infty} \frac{L(\nu)}{h\nu} d\nu}$.

[15] To distinguish this value from the absolute escape fraction obtained using $f_{\rm esc,rel}$ (see Section 6) we indicate it as $f^{\rm H\alpha}_{\rm esc}$.

Table 4
Emissivity-weighted $f_{\rm esc}$ Upper Limits

Redshift	α	$\langle f_{\rm esc} \rangle$	
		$M_{\rm UV,lim} = -13$	$L_{\rm lim} = 0.01 \times L^*$
$z = 1$	-1.5	3.6%	3.4%
	-1.9	4.6%	4.3%
$z = 7$	-2.0	2.7%	2.4%

Note. In Section 7, we measured upper limits to $f_{\rm esc}$ for stacks of Grade A SFGs, sorted and binned according to $M_{\rm UV}$. We apply these limits to measure an *emissivity-weighted* escape fraction, $\langle f_{\rm esc} \rangle$, from three sets of SFGs, with bin widths equal to $\{-15 \leqslant M_1 < -17.7; -17.7 \leqslant M_2 < -18.4; -18.4 \leqslant M_3 < -20.5$ We calculate $\langle f_{\rm esc} \rangle$ at $z = 1$ and $z = 7$ assuming Schechter parameters of the UV-luminosity function: From Dahlen et al. (2007), $\{M^*, \phi^*\} = \{-19.9, 3.99 \times 10^{-3}\}$ and $\alpha = -1.5, -1.9$ From Finkelstein et al. (2015), $\{M^*, \phi^*\} = \{-21.0, 1.86 \times 10^{-4}\}$, and $\alpha = -2.0$.

where ϕ(L) is the Schechter luminosity function (LF).

To measure $\langle f_{\rm esc} \rangle$, we first computed the upper limits on $f_{\rm esc}$ in three equally sized Grade A SFG samples selected on luminosity: $-15.0 > M_{1,\rm UV} > -17.8, -17.8 > M_{2,\rm UV} > 18.5$, and $-18.5 > M_{3,\rm UV} > -20.5$. Here, we include $f_{\rm esc}$ in the integrand to indicate that it varies as a function of UV luminosity, though *within* each of the luminosity bins it is assumed constant. For these three magnitudes ranges, applying the same technique as in Section 7.1, we measure $f_{\rm esc} < 5.6, 3.9, 1.7$ [%] respectively (3σ; see Table 4).

We compute the integral in Equation (6) down to the faintest observed magnitude ($M_{\rm UV} = -15$, which corresponds to $\sim 0.01L^*$ at $z = 1$). To quantify the contribution of the faintest sources, we also extend the limit of integration down to $M_{\rm UV} = -13$ ($0.001L^*$), assuming that the $\langle f_{\rm esc} \rangle$ limit remains constant down to the chosen limit. The resulting values of $\langle f_{\rm esc} \rangle$ limits are reported in Table 4 for $z \sim 1$ and $z \sim 7$, assuming parameters for the LF measured by Dahlen et al. (2007) and Finkelstein et al. (2015), respectively. The emissivity weighted $f_{\rm esc}$ limits presented in Table 4 imply that the observed population of SFGs contribute, on average, less than 50% of the ionizing background at $z \sim 1$.

We note here that the reported upper limits are valid for populations of galaxies, and cannot be used for individual sources. In fact, in calculating $f_{\rm esc}$ we are implicitly assuming that the LyC is radiated away from the galaxy isotropically. The orientation of a galaxy toward the observer's line of sight may affect the identification of LyC—starburst galaxies have been identified with strong winds and outflows which could produce channels through which LyC may "stream" to the IGM (Heckman et al. 2001), though it is useful to note that starburst galaxies with strong winds have not been detected to emit LyC (Grimes et al. 2009). In simulations as well, orientation biases in the identification of LyC candidates are possible. Recently, Kimm & Cen (2015) investigated, via cosmological hydrodynamical simulations, the uncertainty introduced in the measurement of $f_{\rm esc}$ by stacking SFGs in which LyC only escapes through channels with narrow opening angles. In this work, we have stacked samples of *hundreds* of galaxies to derive the upper limits; Kimm & Cen show that for such large samples, the *uncertainty* on $f_{\rm esc}$ is $\lesssim$20%.

9. DISCUSSION

Previous reports of the non-detection of escaping LyC in deep imaging of $z \sim 1$ SFGs, which necessarily produce LyC photons, imply that some physical process(es) prevents this ionizing emission from escaping to the IGM. In the previous section, we considered in a novel way the escape of LyC from groups of galaxies defined with broadly similar physical characteristics (e.g., morphology, star formation history) as measured from multi-wavelength UV-optical, high spatial resolution imaging, and grism spectroscopy. A detection of escaping LyC from galaxies in any of these groups could indicate that particular physical process(es) are more likely to promote the escape of LyC from SFGs. However, for all all groups we measure only *upper limits* to $f_{\rm esc}$.

The direct detection of the LyC escape fraction in $z \sim 1$ SFGs is not essential to explain reionization at low redshift, because in this redshift range, SFGs are the sub-dominant contributor to the ionizing UV background. The upper limits to $f_{\rm esc}$ presented here are more useful for constraining the contribution of the *analogs* of SFGs at redshift $z > 4$. Although there are no constraints on the characteristics (e.g., mass, luminosity, metallicity) of LyC emitters at $z > 4$, observations and simulations suggest that the selection criteria applied in Section 4 should identify low-redshift analogs to the sources of reionization. For example, the low-luminosity and low-mass galaxy sub-samples are measured to have a mean $M_{\rm UV} \simeq -16.5$. At $z \sim 7$, this is equivalent to $L \simeq 0.02L^*$. These and lower-luminosity dwarf galaxies are inferred form high redshift surveys to be critical sources of re-ionizing photons (e.g., Robertson et al. 2015). Here, we discuss the implications of these measured upper limits for reionization of the IGM at high redshift ($z \sim 7$).

At high redshift, the high column density of neutral absorbers prevents the direct detection of LyC. Thus, the contribution of high redshift SFGs to reionization is inferred from the observable non-ionizing UV luminosity density ($\rho_{\rm UV}$). Specifically, $\rho_{\rm UV}$ can be related to the escape of ionizing photons following Madau et al. (1999), which Finkelstein et al. (2012) update as

$$\rho_{\rm UV} = 1.24 \times 10^{25} \cdot \epsilon_{53}^{-1} \left(\frac{1+z}{8}\right)^3 \left(\frac{\Omega_b\, h_{70}^2}{0.0461}\right)^2 x_{\rm H\,II,z} \cdot \frac{C}{f_{\rm esc}} [\rm erg\ s^{-1}\ Hz^{-1}\ Mpc^{-3}] \quad (7)$$

where ϵ_{53} is the number of Lyman continuum photons per unit of forming stellar mass, in units of 10^{53} photons $\rm s^{-1}$, $x_{\rm H\,II,z}$ is the volume averaged fraction of ionized hydrogen at redshift z, and C is the ionized hydrogen gas clumping factor)[16] in the IGM ($C = \langle n^2 \rangle / \langle n \rangle^2$). Here, the prefactor results from equilibrating the volume averaged rate at which ionized photons from young, hot stars are are emitted into the IGM with the recombination rate of neutral gas in the IGM.

With reasonable assumptions to $x_{\rm H\,II,z}$ and the clumping factor, we calculate the theoretical UV luminosity density for comparison with high redshift observations. In this calculation, we will assume $f_{\rm esc}$ at $z = 7$ equals to $\langle f_{\rm esc} \rangle < 2.7\%$, which is the upper limit we measured in Section 8 for $z \sim 1$ SFGs integrated over a comparable range of luminosity to allow for a direct comparison with calculations of $\rho_{\rm UV}$ measured at high redshift (e.g., Finkelstein et al. 2015; Robertson et al. 2015). We discuss the validity of this assumption following the calculation. Assuming a clumping factor typical for the high-redshift universe, $C \sim 3$, $\epsilon_{53} \simeq 1$, and $f_{\rm esc} < 2.7\%$, then to *critically* reionize the IGM at $z \sim 7$ ($x_{\rm H\,II} = 1$) requires $\rho_{\rm UV} \gtrsim 1.3 \times 10^{27}\ \rm erg\ s^{-1}\ Hz^{-1}\ Mpc^{-3}$. From direct observations reported in Finkelstein et al. (2015), integrating the UV LF measured at $z \sim 7$ over the range $M_{\rm UV} = [-13, -23]$, $\rho_{\rm UV} \sim 1.3 \times 10^{26}\ \rm erg\ s^{-1}\ Hz^{-1}\ Mpc^{-3}$.Thus, SFGs fail to meet the threshold for critical reionization at $z \sim 7$ by an *order of magnitude*.

Implicit in this calculation are two noteworthy assumptions. First, we assume that $f_{\rm esc,z=1} = f_{\rm esc,z=7}$. Multiple groups have measured a strong positive evolution of the escape fraction of Lyα with increasing redshift (Hayes et al. 2011; Kuhlen & Faucher-Giguére et al. 2012). It is reasonable to expect the escape of LyC photons to be proportional to that of Lyα photons (e.g., Verhamme et al. 2015) therefore we may expect the escape of LyC photons may increase with redshift. Second, the neutral fraction at $z \sim 7$ may in fact be non-zero, i.e., reionization is not fully complete until lower redshift ($z \lesssim 6$). Observations of a rapid evolution of Lyα emitters between $z \sim 6$–7 suggest $0.2 \lesssim x_{\rm H\,II,z} \lesssim 0.6$ (see Pentericci et al. 2011). Thus, if the escape fraction evolves with redshift or the volume averaged fraction of ionized hydrogen is lower than was assumed here, the disparity between the observed and predicted UV luminosity density would be reduced and SFGs brighter than $M_{\rm UV} < -13$ could in principle maintain reionization at $z \sim 7$.

It is interesting to compare what an $f_{\rm esc} = 2.7\%$ would imply for $\tau_{\rm es}$, the Thomson scattering optical depth of CMB photons by free electrons along the line of the sight (see, e.g., Nolta et al. 2009). New results from the Planck Collaboration have revised the value of $\tau_{\rm es}$ downward to $\tau_{\rm es} = 0.063 \pm 0.012$ (Planck Collaboration et al. 2015). Robertson et al. (2015) recently demonstrated that this revised value of $\tau_{\rm es}$ can be reproduced assuming $f_{\rm esc} \sim 20\%$ and integrating the contribution of SFGs as faint as $L = 0.001L^*$, while Finkelstein et al. (2015) also found $\tau_{\rm es}$ remains consistent with the Planck measurement even if $f_{\rm esc}$ assumed for such faint SFGs is as low as $f_{\rm esc} = 13\%$. Using $\rho_{\rm UV}(z)$ calculated and compiled by Finkelstein et al. (2015) for SFGs brighter than a limiting luminosity $L = 0.001L^*$, and assuming a *constant* $f_{\rm esc} < 2.7\%$ over the redshift range $4 < z < 11$ and $C = 3$, we can infer an ionization history over this redshift range directly from Equation (7). From this redshift-dependent ionization history, we compute an upper limit to $\tau_{\rm es} < 0.059$ (3σ). This $\tau_{\rm es}$ remains marginally consistent (at 1σ) with the latest measurement of $\tau_{\rm es}$ by the Planck Collaboration.

Finally, we note that the pressure to accomodate reionization at high redshift *exclusively* with emission from SFGs has been recently called into question. Giallongo et al. (2015) recently identified 22 low-luminosity $4 < z < 6$ AGNs in the GOODS-S field—35% of which were not previously reported—and suggested that the ionizing continuum from such objects *alone* provides a dominant contribution to the reionization at high redshift. Similarly, Madau & Haardt (2015) reconsider the ionization history of hydrogen and helium in an AGN-dominated scenario and predict $\tau_{\rm es} = 0.055$, which is similar

[16] A clumping factor equal to unity corresponds to a homogenous medium. In simulations, the range of clumping factors typically assumed equals $1 \lesssim C \lesssim 50$ (Gnedin & Ostriker 1997; Pawlik et al. 2009; Finlator et al. 2012).

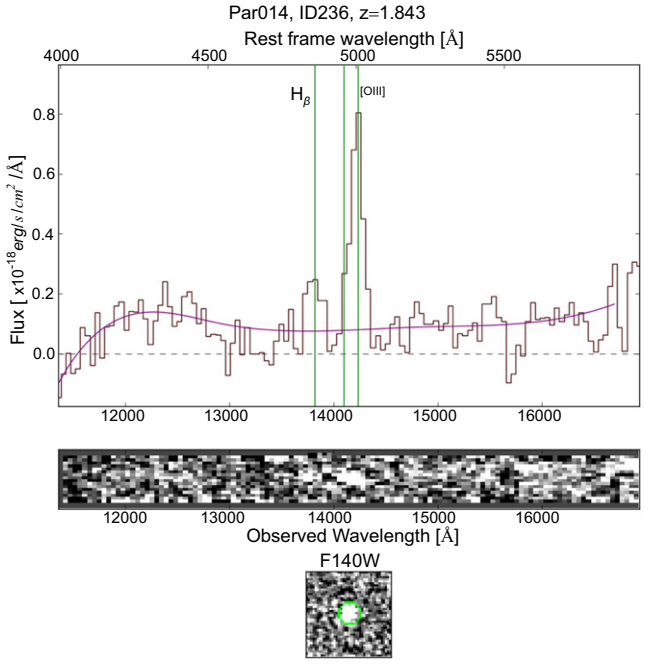

Figure 6. Representative galaxy (<5% of all SFGs) for which the photometric redshift disagrees significantly with the measured spectroscopic redshift and can not be attributed to a mis-attribution of an emission-line(s). Here, Hβ and the unresolved [O III] doublet are clearly identified in the one- and two-dimensional spectra, implying the spectroscopic redshift is correct.

to our upper limit derived for τ_{es} derived for a reionization history dominated by stellar sources of the hydrogen-ionizing emission in Figure 6. In contrast, Haardt & Salvaterra (2015) measure τ_{es} to be a factor of 2 *larger* than the recent Planck result when allowing for a larger population of obscured AGNs than Madau & Haardt (2015). Regardless, considering the fact that we do not detect escaping LyC emission in the stacked photometry of $\sim 10^3$ SFGs, this AGN-dominated scenario is appealing and in future work we will directly address this question using these *GALEX* and *HST* data.

10. CONCLUSION

Combining publicly available multi-wavelength archival data from multiple deep imaging and spectroscopic surveys, we have made a renewed search for escaping Lyman continuum emission in star-forming galaxies at $z \sim 1$. We select star-forming galaxies from catalogs of ELGs prepared from an independent reduction of *HST* WFC3 imaging and G141 grism data obtained originally as part of the 3DHST and AGHAST suveys. Initially, we produced a large ($N \sim 1400$) sample of SFGs at $0.9 < z < 1.4$ identified as such by the presence of Hα in emission. We apply a two-tiered selection against galaxies in this initial sample to strongly exclude SFGs that could potentially suffer photometric contamination from unresolved sources in the lower spatial resolution *GALEX* images. The final sample ("Grade A") contained ~600 SFGs, and was used primarily for all analysis. We find no unambiguous evidence for escaping LyC in individual galaxies. Thus, we stacked all galaxies in each sample and, using the optical photometry compiled by the 3DHST team for the fields, derived 3σ upper limits to f_{esc} equal ~2%. In particular, we sub-divided the Grade A sample on the basis of SFG's stellar mass, inclination and Hα equivalent width and report their associated upper limits. In particular, we measured an upper limit of $f_{esc} \lesssim 9.6\%$ for "extreme emission line" (H$\alpha > 200$ Å) galaxies.

In addition, we have used an emissivity-weighted upper limit, $\langle f_{esc} \rangle$, to constrain the contribution of SFGs to the ionizing UV background near to the end of the reionization ($z \sim 7$). This f_{esc} upper limit was measured for $z \sim 1$ SFGs, which we assume to be reasonable analogs to the high redshift sources of ionizing photons. If the escape fraction of $z \sim 7$ SFGs brighter than $M_{UV} \sim -13$ is less than $\langle f_{esc} \rangle \sim 2.7\%$, the ionizing emissivity of these SFGs is insufficient to *critically* reionize the high redshift universe. If the LyC escape fraction increases with redshift, SFGs remain plausible candidates for reionization at high redshift and marginally consistent with results from Planck, though we note that SFGs fainter than $M_{UV} > -17$ are not observed in current surveys of the high redshift universe. Alternatively, the contribution from an additional source (potentially low-luminosity AGNs) of ionizing photons could sustain reionization during the Epoch of Reionization beginning at $z > 11$ and completed by $z \sim 4$–6.

We thank the referee, B. Robertson, for helpful comments that improved the discussion and conclusions presented in this work. We also thank S. Finkelstein for helpful discussion. M.H. acknowledges the support of the Swedish Research Council (Vetenskapsrådet), the Swedish National Space Board (SNSB), and the Knut and Alice Wallenberg Foundation. This research was supported by NASA NNX13AI55G and *HST*-AR Program #12821.01, using observations taken by the 3D-HST Treasury program (GO 12177 & 12328) with the NASA/ESA *HST*, which is operated by the Association of Universities for Research in Astronomy, Inc., under NASA contract NAS5-26555. *GALEX* and *HST* data presented in this paper were obtained from the Mikulski Archive for Space Telescopes (MAST) maintained by the STScI. Support for MAST for non-*HST* data is provided by the NASA Office of Space Science via grant NNX13AC07G and by other grants and contracts. This research has made use of NASA's Astrophysics Data System Bibliographic Services.

APPENDIX A
THE ACCURACY OF z_{spec} DERIVED FROM G141 EMISSION-LINE SPECTRA

In general, we find good agreement between the photometric redshifts reported in Skelton et al. (2014) and the grism spectroscopic redshifts we used here—$\Delta(z) = \frac{z_{spec} - z_{phot}}{1 + z_{phot}} < 5\%$ for ~50% of all ELGs (2307/4481).

We can improve the agreement between photometric and spectroscopic redshifts to ~70% by using the photometric redshift as a prior to correct for mis-classified emission lines for which only a single emission line was observed in the G141 spectrum. The inspection of a spectrum obtained with a single grism is strongly susceptible to the mis-classification of emission lines when only a *single line* is observed. By default, we classified such emission lines as Hα and *not* a similarly bright, nebular emission line blue-ward of Hα ([O II]λ3727 Å] [O III]$\lambda\lambda$4959, 5007 Å]), or other possibly prominent lines red-ward of Hα (He Iλ10830 Å, or the recombination Paschen series). Only in rare instances could the morphology of the single emission line (i.e., a blue "wing" in an unresolved [O III] doublet) be used to overrule the default classification, but unless both inspectors agreed to this classification after second

inspection these galaxies would not be included in our sample as we require both independent classifications of the emission line to agree for ELG selection. Fortunately, extensive imaging of these fields provides a long wavelength baseline for the measurement of accurate photometric redshifts. We apply the 3DHST collaboration's public photometric redshift catalogs as a prior to constrain the "true" redshift for ~800 ELGs (red circles of Figure 4) whose spectra displayed only a single emission line. This correction marginally improves the size (~10%) of the catalog of $0.9 < z < 1.4$ EFGs for which the G141 is sensitive to the rest-frame Hα emission.

Robust photometric redshifts are essential for the confirmation of emission lines identified in grism surveys, but these measurements can be incorrect as well. For a small subset of the galaxies ($N = 64$), the redshift discrepancy can be attributed to incorrect *photometric* redshifts. In these EFGs, the emission line was cataloged as [O III] by inspection, implying a spectroscopic redshift $1.7 \lesssim < z < 2.2$, but the photometric redshift is ~30% lower. An example is provided in Figure 6; this EFG clearly displays multiple strong emission lines of Hβ and [O III], which is unresolved in the G141 grism. In Figure 6, the 1D, 2D grism spectra, and the F140W direct image of galaxy is provided; here, the direct image is aligned with the orientation of the dispersion axis in the grism. Using the correct spectroscopic redshift for these EFGs places them beyond the range of interest, $0.9 < z < 1.4$, thus we excluded these galaxies from our analysis. We include these galaxies in the public catalogs we have made available online.

APPENDIX B
THE SOURCES OF ADDITIONAL DISCREPANCIES BETWEEN $z_{\rm spec}$ AND $z_{\rm phot}$

We observe a significant ($\Delta(z) > 5\%$) discrepancy between the 3DHST photometric redshift and the spectroscopic redshift for a minority (~30%) of ELGs. This discrepancy can not be corrected for using a photometric redshift prior as discussed in Appendix A. In this section, we discuss three likely scenarios that give rise to these discrepancies.

First, we investigate ~150 $z_{\rm spec} \simeq 1.2$ single-emission line EFGs whose discrepant redshifts could not be associated with a mis-classified single emission ([O III] was mis-classified as Hα) in single emission-line spectra. Approximately 10% of these galaxies are observed to be spatially near to ($\ll$1 arcsec), or blended with, a neighboring galaxy. Automated photometry measurement software will have some difficulty in distinguishing closely separated sources. In some instances, the detection deblending parameters can be fine-tuned to reduce source confusion (see, e.g., recent work with the UVUDF; Rafelski et al. 2015) of close pairs or mergers in which the system can be resolved as two distinct galaxies, but ultimately the photometry will be contaminated in the close pair system. Such galaxies are only a small fraction of all ELGs, thus the flux blending due to source confusion is likely to be only a minor factor in the redshift discrepancy for the full sample.

Second, and more importantly, we noted in visual inspection that most of these galaxies (~70%) are faint ($m \lesssim 24$) and compact ($r_e \sim 3$ pixels) in the direct image. This raises the possibility that the emission line, attributed as Hα, could contribute significantly to the broad-band magnitude (see, e.g., Atek et al. 2014) and thus affect the measurement of the photometric redshift. In Figure 7 we measure the contribution of the observed emission line to the observed magnitude in the F140W filter. Here, a two-dimensional histogram of galaxies with correctly identified Hα (i.e., $\frac{z_{\rm spec} - z_{\rm phot}}{1 + z_{\rm phot}} < 5\%$)—are over-plotted. Red data indicate those galaxies that have discrepant redshifts.

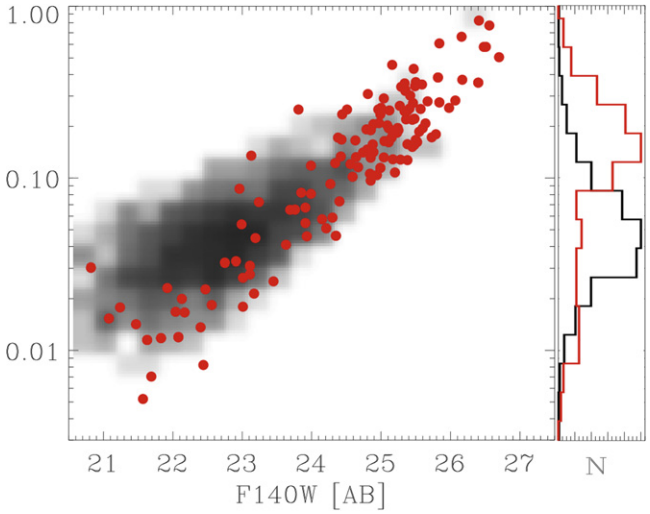

Figure 7. We measured the contribution of the Hα emission line to the broadband F140W photometry, presented here as a percentage of the total flux, for two subsets of SFGs. Gray, binned data indicates SFGs with grism spectroscopic redshifts in good agreement with published 3DHST photometric redshifts. Red data indicate $z \sim 2$ SFGs with single emission lines and discrepant redshifts, but whose lines could not be re-classified from Hα to [O III] using the photometric redshift as prior on the classification. The two distributions are clearly offset; here, the SFGs with discrepant photometric redshifts can here be attributed to the contribution of strong emission from a high EW Hα.

In Figure 7, there is a clear distinction in the centroids of the distribution of the gray-scale (all galaxies) and discrete, red (strong contribution of Hα to the continuum flux) data. The contribution from line emission (>10%, and extending to nearly 100%) to the broadband F140W magnitude can affect the SED of the galaxy (~0.5 mag Atek et al. 2011) and thus the inferred physical characteristics (see, e.g., de Barros et al. 2014) and photometric redshift. If the IR photometry is affected by strong Hα, additional nebular lines may too be bright and the galaxy's broadband SED at shorter rest-frame wavelengths may also be adversely affected. In the case where strong emission lines are observed in faint ELGs, we take a conservative approach and choose to exclude these galaxies from the Grade A/B sample. If the mis-classified emission line is associated with a galaxy at lower ($z \lesssim 0.9$) redshift, flux in the *GALEX* FUV filter would be associated with the non-ionizing continuum and these sources would contaminate the measurement of the $f_{\rm esc}$.

Third, we consider those EFGs identified at $0.9 < z_{\rm spec} < 1.4$, but $0 < z_{\rm phot} < 0.9$. In this sub-sample, the Hα emission line contributes $\gtrsim$10% of the total flux in the broadband filter in only ~30% of the galaxies, thus the accuracy in the measured photometric redshift is not singularly at issue. Instead, we attribute the redshift discrepancy measured for this subset of galaxies to at least one of four additional issues. First, nearly half of all sources were measured with an Hα equivalent width less than 40 Å, making the positive

identification by eye more difficult in galaxies with fainter continuua. *HST* grism surveys are largely incomplete to such low EW sources (Colbert et al. 2013) and we removed sources with such low EWs from our sample selection in Section 3 but discuss them here for completeness. Of the remaining 55% of sources with a redshift discrepancy $\Delta(z) > 5\%$, ~50% of these galaxies among the brightest studied ($m_{\rm F140W} < 23$) and their grism spectra were correspondingly dominated by a very bright continuum spectral profile, which made it difficult to visually confirm the presence of an emission line. A visual inspection of all galaxies direct image also confirms that approximately 50% of all galaxies were large spiral galaxies. These observations suggest that the photometric redshifts are indeed accurate and the discrepancy in redshifts is likely attributable to an incorrectly measured spectroscopic redshifts. We attempted to confirm the accuracy of the photometric redshifts for these galaxies, assuming the candidate emission line was associated with near-IR emission lines of He I and the Paschen series but these results were inconclusive as often only a single emission line was identified in the grism spectra. Among the full sample of these low-redshift discrepant ELGs, we attribute an additional 50% (for a total of ~100%, including the bright continuum and spiral galaxies) of redshift discrepancies to contamination issues. Sources of contamination included (1) overlapping 1*st* (or higher) order spectra in the extracted spectra from galaxies in pairs, groups, or in close proximity to bright galaxies (~60%) and (2) noise arising from the proximity of the dispersed spectrum to either the dead pixel region[17] or near the edge of the IR detector (~40%). We elect not to correct the redshifts for these galaxies—if the photometric redshift is incorrect, the *GALEX* FUV filter would be sensitive to significant non-ionizing UV continuum which would contaminate the measurement of $f_{\rm esc}$.

REFERENCES

Alexander, D. M., Bauer, F. E., Brandt, W. N., et al. 2003, AJ, 126, 539
Amorin, R., Sommariva, V., Castellano, M., et al. 2014, A&A, 568, L8
Atek, H., Kneib, J.-P., Pacifici, C., et al. 2014, ApJ, 789, 96
Atek, H., Malkan, M., McCarthey, P., et al. 2010, ApJ, 723, 104
Atek, H., Richard, J., Kneib, J.-P., et al. 2015, ApJ, 800, 18
Atek, H., Siana, B., & Scarlata, C. 2011, ApJ, 743, 121
Becker, R. H., Fan, X., White, R. L., et al. 2001, AJ, 122, 2850
Bergvall, N., Zackrisson, E., Andersson, B.-G., et al. 2006, A&A, 448, 513
Bertin, E., & Arnouts, S. 1996, A&AS, 117, 393
Borthakur, S., Heckman, T., Leitherer, C., & Overzier, R. 2014, Science, 346, 216
Brammer, G., van Dokkum, P. G., Franx, M., et al. 2012, ApJS, 200, 13
Bridge, C., Teplitz, H. I., Siana, B., et al. 2010, ApJ, 720, 465
Bruzual, A. G., & Charlot, S. 2003, MNRAS, 344, 1000
Calzetti, D., Armus, L., Bohlin, R., et al. 2000, ApJ, 533, 682
Cardelli, J. A., Clayton, G. C., & Mathis, J. S. 1989, ApJ, 345, 245
Chabrier, G. 2003, PASP, 115, 809
Colbert, J., Teplitz, H., Atek, K., et al. 2013, ApJ, 779, 34
Cowie, L., Barger, A. J., & Hu, E. M. 2011, ApJ, 738, 136
Cowie, L., Barger, A. J., & Trouille, L. 2009, ApJ, 692, 1476 (CBT09)
Dahlen, T., Mobasher, B., Dickinson, M., et al. 2007, ApJ, 654, 172
de Barros, A., Vanzella, E., Amorín, R., et al. 2016, A&A, 585, A51
de Barros, S., Schaerer, D., & Stark, D. P. 2014, A&A, 563, A81
Djorgovski, S. G., Castro, S., Stern, D., et al. 2001, ApJL, 560, L5
Dominguez, A., Siana, B., Brooks, A. M., et al. 2014, MNRAS, 451, 1
Dominguez, A., Siana, B., Brooks, A. M., et al. 2015, MNRAS, 451, 839
Dominguez, A., Siana, B., Henry, A., et al. 2013, ApJ, 763, 145
Dopita, M., Krauss, L. M., Sutherland, R. S., et al. 2011, A&SS, 335, 345
Ekström, S., Georgy, C., Eggenberger, P., et al. 2012, A&A, 537, A146
Erb, D., Shapley, A. E., Pettini, M., et al. 2006, ApJ, 644, 813

[17] The "Death Star," see *HST* IR Instrument Science Report #WFC3-2008-28.

Fan, X., Narayanan, V. K., Strauss, M. A., et al. 2002, AJ, 123, 1247
Fan, X., Strauss, M. A., Becker, R. H., et al. 2006, AJ, 132, 117
Faucher-Giguére, C.-A., Lidz, A., Hernquist, L., & Zaldarriaga, M. 2008, ApJ, 688, 85
Finkelstein, S. L., Papovich, C., Ryan, R. E., et al. 2012, ApJ, 758, 93
Finkelstein, S. L., Ryan, R. E., Jr., Papovich, C., et al. 2015, ApJ, 810, 71
Finlator, K., Oh, S. P., Özel, F., & Davé, R. 2012, MNRAS, 427, 2464
Fujita, A., Martin, C. L., Mac Low, M.-M., & Abel, T. 2003, ApJ, 599, 50
Giallongo, E., Grazian, A., Fiore, F., et al. 2015, A&A, 578, A83
Gnedin, N. ,Y., & Ostriker, J. P. 1997, ApJ, 486, 581
Gonzaga, S., Hack, W., Fruchter, A., & Mack, J. (ed.) 2012, The DrizzlePac Handbook (Baltimore: STScI), 53
Grimes, J. P., Heckman, T., Aloisi, A., et al. 2009, ApJS, 181, 272
Grimes, J. P., Heckman, T., Strickland, D., et al. 2007, ApJ, 668, 891
Haardt, F., & Madau, P. 1996, ApJ, 461, 20
Haardt, F., & Madau, P. 2012, ApJ, 746, 125
Haardt, F., & Salvaterra, R. 2015, A&A, 575, L16
Hammer, D., Hornschemeier, A. E., Mobasher, B., et al. 2007, ApJS, 190, 43
Hayes, M., Schaerer, D., Östlin, G., et al. 2011, ApJ, 730, 8
Heckman, T., Borthakur, S., Overzier, R., et al. 2011, ApJ, 730, 5
Heckman, T., Sembach, K. R., Meurer, G. R., et al. 2001, ApJ, 558, 56
Henry, A., Scarlata, C., Martin, C. L., et al. 2015, ApJ, 809, 25
Hinshaw, G., Larson, D., Komatsu, E., et al. 2013, ApJS, 208, 19
Inoue, A. K. 2002, ApJL, 570, L97
Inoue, A. K., & Iwata, I. 2008, MNRAS, 387, 1681
Inoue, A. K., Shimizu, I., Awata, I., et al. 2014, MNRAS, 442, 1805
Iwata, I., Inoue, A. K., Matsuda, Y., et al. 2009, ApJ, 692, 1287
Kimm, T., & Cen, R. 2015, ApJL, 801, L25
Komatsu, E., Smith, K. M., Dunkley, J., et al. 2011, ApJS, 192, 18
Kuhlen, M., & Faucher-Giguére, C. A. 2012, MNRAS, 423, 862
Laird, E. S., Nandra, K., Georgakakis, A., et al. 2009, ApJS, 180, 102
Lee, J. C., Gil de Paz, A., Tremonti, C., et al. 2009, ApJ, 706, 599
Leitet, E., Bergvall, N., Hayes, M., et al. 2013, A&A, 553, A16
Leitet, E., Bergvall, N., Piskunov, N., & Andersson, B.-G. 2011, A&A, 532, A107
Leitherer, C., Ekstr'om, S., Meynet, G., et al. 2014, ApJS, 212, 14
Leitherer, C., Ferguson, H. C., Heckman, T. M., & Lowenthal, J. D. 1995, ApJL, 454, L19
Leitherer, C., Schaerer, D., & Goldader, J. D. 1999, ApJS, 123, 3
Levesque, E., Leitherer, C., Ekström, S., et al. 2012, ApJ, 751, 67
Loeb, A., & Barkana, R. 2001, ARA&A, 39, 19
Madau, P., & Haardt, F. 2015, ApJL, 813, L8
Madau, P., Haardt, F., & Rees, M. 1999, ApJ, 514, 648
Malkan, M., Webb, W., & Konopacky, Q. 2003, ApJ, 598, 878
Maller, A. H., Berlind, A. A., Blanton, M. R., et al. 2009, ApJ, 691, 394
Maraston, C. 2005, MNRAS, 362, 799
Martin, C., Barlow, T., Barnhart, W., et al. 2003, Proc. SPIE, 336, 4854
McGreer, I. D., Mesinger, A., & D'Odorico, V. 2014, MNRAS, 447, 499
Morrissey, P., Conrow, T., Barlow, T. A., et al. 2007, ApJS, 173, 682
Mostardi, R. E., Shapley, A. E., Nestor, D. B., et al. 2013, ApJ, 778, 65
Mostardi, R. E., Shapley, A. E., Steidel, C. C., et al. 2015, ApJ, 810, 107
Nestor, D. B., Shapley, A. E., Kornei, K. A., et al. 2014, ApJ, 765, 47
Nestor, D. B., Shapley, A. E., Steidel, C. C., et al. 2011, ApJ, 736, 18
O'Donnell, J. E. 1994, ApJ, 422, 158
Oke, J. B., & Gunn, J. E. 1983, ApJ, 266, 713
Osmer, P. S. 1982, ApJ, 253, 28
Pawlik, A. H., Schaye, J., & van Scherpenzeel, E. 2009, MNRAS, 394, 1812
Pentericci, L., Fontana, A., Vanzella, E., et al. 2011, ApJ, 743, 132
Planck Collaboration, Ade, P. A. R., Aghanim, N., et al. 2015, arXiv:1502.01589
Rafelski, M., Teplitz, H. I., Gardner, J. P., et al. 2015, ApJ, 150, 31
Rauch, M., Miralda-Escudé, J., & Sargent, W. L. W. 1997, ApJ, 489, 7
Razoumov, A. O., & Sommer-Larsen, J. 2006, ApJL, 651, L89R
Robertson, B. E., Ellis, R. S., Furlanetto, S. R., & Dunlop, J. S. 2015, ApJL, 802, L19
Ross, N. L., Malkan, M., Rafelski, M., et al. 2015, ApJ, submitted
Salpeter, E. E. 1955, ApJ, 121, 161
Salvato, M., Ilbert, O., Hasinger, G., et al. 2011, ApJ, 742, 61
Schaerer, D. 2003, A&A, 397, 527
Schlegel, D. J., Finkbeiner, D. P., & Davis, M. 1998, ApJ, 500, 525
Schleicher, D. R. G., Banerjee, R., & Klessen, R. S. 2009, PhRvD, 79, 043510
Siana, B. 2005, PhD thesis, Univ. California, San Diego
Siana, B., Shapley, A. E., Kulas, K., et al. 2015, ApJ, 804, 17
Siana, B., Teplitz, H. I., Colbert, J., et al. 2007, ApJ, 668, 62
Siana, B., Teplitz, H. I., Ferguson, H. C., et al. 2010, ApJ, 723, 241

Skelton, R., Whitaker, K. E., Momcheva, I. G., et al. 2014, ApJS, 214, 24
Steidel, C. C., Pettini, M., & Adelberger, K. L. 2001, ApJ, 546, 665
van der Burg, R. F. J., Muzzin, A., Hoekstra, H., et al. 2013, A&A, 557, A15
Verhamme, A., Orlitová, I., Schaerer, D., & Hayes, M. 2015, A&A, 578, A7
Weymann, R., Jannuzi, B. T., Lu, L., et al. 1998, ApJ, 506, 1
Wise, J. H., Demchenko, V. G., Halicek, M. T., et al. 2014, MNRAS, 442, 2560
Wuyts, S., Förster Schreiber, N. M., van der Wel, A., et al. 2011, ApJ, 738, 106
Zaroubi, S., Thomas, R. M., Sugiyama, N., & Silk, J. 2007, MNRAS, 375, 1269